Wide range strain distributions on the electrode for a highly sensitive flexible tactile sensor with low hysteresis

Journal:	*ACS Applied Materials & Interfaces*
Manuscript ID	am-2022-21241x.R1
Manuscript Type:	Article
Date Submitted by the Author:	n/a
Complete List of Authors:	Liang, Cuiyuan; Harbin Institute of Technology Sun, Jingqi ; Harbin Institute of Technology Liu, Zhihua; Nanyang Technological University Tian, Gongwei; Harbin Institute of Technology School of Chemistry and Chemical Engineering Liu, Yan; Harbin Institute of Technology Zhao, Qinyi; Harbin Institute of Technology School of Chemistry and Chemical Engineering Yang, Dan ; Harbin Institute of Technology Chen, Jianhui; Harbin Institute of Technology School of Chemistry and Chemical Engineering Zhong, Bowen ; Harbin Institute of Technology Zhu, Ming; Harbin Institute of Technology School of Chemistry and Chemical Engineering Xu, Hongbo; Harbin Institute of Technology Qi, Dianpeng; Harbin Institute of Technology

Wide range strain distributions on the electrode for a highly sensitive flexible tactile sensor with low hysteresis

Cuiyuan Liang[a], Jingqi Sun[a], Zhihua Liu[b], Gongwei Tian[a], Yan Liu[a], Qinyi Zhao[a], Dan Yang[a], Jianhui Chen[a], Bowen Zhong[a], Ming Zhu[a], Hongbo Xu[a], and Dianpeng Qi[a]**

a. National and Local Joint Engineering Laboratory for Synthesis, Transformation and Separation of Extreme Environmental Nutrients; MIIT Key Laboratory of Critical Materials Technology for New Energy Conversion and Storage, School of Chemistry and Chemical Engineering, Harbin Institute of Technology, Harbin 150001, P. R. China.

b. Institute of Materials Research and Engineering, Agency for Science, Technology and Research (A*STAR), 138634, Singapore.

*Corresponding authors: Dianpeng Qi (E-mail: dpqi@hit.edu.cn), Yan Liu (E-mail: liuyan1986@hit.edu.cn)

ABSTRACT: Flexible piezoresistive tactile sensors are widely used in wearable electronic devices because of their ability to detect mechanical stimuli. However, achieving high sensitivity and low hysteresis over a broad detection range remains a challenge with current piezoresistive tactile sensors. To address these obstacles, we designed elastomeric micropyramid arrays with different heights to redistribute the strain on the electrode. Furthermore, we mixed single-walled carbon nanotubes in the elastomeric micropyramids to compensate for the conductivity loss caused by random cracks in the gold film and increase the adhesion strength between the gold film (deposited on the pyramid surface) and the elastomer. Thus, the energy loss of the sensor during deformation and the hysteresis (~2.52%) were effectively reduced. Therefore, under the synactic effects of the percolation effect, tunnel effect, and multistage strain distribution, the as-prepared sensor exhibited a high sensitivity (1.28×10^6 kPa^{-1}) and a broad detection range (4.51–54837.06 Pa). The sensitivity was considerably higher than those of most flexible pressure sensors with a microstructure design. As a proof of concept, the sensors were successfully applied in the fields of health monitoring and human–machine interaction.

KEYWORDS: sensor, pyramid, two conductive paths, health monitoring, human–machine interaction

1. Introduction

With the rapid advancement and increasing demands for human–computer interaction, health monitoring, and soft robots, the study of flexible tactile sensors has recently increased.[1-3] Among the various flexible tactile sensors with different sensing mechanisms (e.g., piezoresistive, capacitive, optical, magnetic, *etc.*),[4-10] piezoresistive soft tactile sensors have attracted extensive attention because of their simple structure, easy fabrication, low cost, and straightforward output principle (the external pressure is converted into a recognizable electrical signal).[11] To a certain extent, flexible tactile sensors can help inanimate objects recognize the "feel" of their interactions with humans and gain real-time information about human physiology and activities.[12] To perform these functions, piezoresistive tactile sensors must possess high sensitivity and low hysteresis over a wide detection range.

High-sensitivity sensors with a wide detection range are indispensable in a variety of scenarios, including detection of intraocular pressure and pulse (<1 kPa), mimicking the ability of the human body to sense touch (1–10 kPa), and manipulating objects (>10 kPa). As a result, maintaining high sensitivity and a wide detection range in flexible pressure sensors is critical for practical applications. However, high sensitivity and a wide detection range have an inherent trade-off effect.[13] At present, most strategies for overcoming the sensitivity limit of soft tactile sensors are focused on building microstructures on an elastomer substrate (e.g., polydimethylsiloxane (PDMS), Ecoflex, polyurethane, *etc.*).[14-15] For piezoresistive pressure sensors, elastomer microstructures must be conductive. Normally, carbon-based materials (reduced graphite oxide and carbon nanotubes[16-18]), conductive polymers (poly(3,4-ethylenedioxythiophene)[19] and polypyrrole[20]), or metal materials (silver nanoparticles and gold (Au))[21] are added to the surface or inside the elastomer microstructures to provide conductivity. The pyramid structure is the most commonly used microstructure because of the uneven stress distribution on the pyramid, which is primarily concentrated at the tip (**Figure S1a, Supporting Information (SI)**). Compared with flat surfaces, the higher local stress concentration promotes greater variation in the contact area between the two electrodes of the sensor. Therefore, the resistance change is enhanced, representing high sensitivity.[11] Recently, a porous pyramidal microstructure[22] (**Figure S1b, SI**) and a micropyramid structure with metal ring cracks[23] (**Figure S1c, SI**) were created to further improve the sensitivity of the sensor; however, the sensing capability reached saturation in the low-pressure range (<20 kPa). Therefore, achieving both high sensitivity and a wide pressure detection range in flexible tactile sensors remains a challenge (**Figure S2, SI**).

In addition, sensors with low hysteresis can be utilized to prevent signal distortion and for accurate dynamic monitoring of human motion. Achieving low hysteresis remains a challenge for the flexible tactile sensor. Viscoelastic substrates always cause hysteresis owing to internal energy loss (irreversible frictional energy loss in the polymer chain caused by cyclic deformation) and external energy loss (caused by friction and adhesion at the interface of the two electrodes). Hysteresis caused by external energy loss can be effectively reduced by creating microstructures (e.g., porous structures,[24] wave-patterned structures,[25] and pyramids[16, 26]) in the active layer of the sensor. For example, the hysteresis of a pollen-shaped hierarchical sensor was only 4.6%.[27] In addition, deposition/sputtering of a metal film on the surface of an elastomer can effectively avoid direct contact between the elastomer and the electrode, thereby further reducing the energy loss and decreasing hysteresis. However, metal films deposited on the microstructures are prone to random cracks and wear when an external force is applied,[28-29] which not only consumes energy and causes hysteresis to increase again but also reduces the reliability of the sensor. Therefore, it is essential to reduce the hysteresis of the sensor.

In this study, to effectively address the trade-off between high sensitivity and a wide pressure detection range, we rationally designed a micropyramid array with different heights (MADH) to redistribute the strain on the active electrode of the sensor in a multistage manner (**Figure S1d, SI**). This was accomplished through a simulation analysis of the sensitivity and response range of the sensors fabricated with different micropyramid arrays. The as-prepared pressure sensor exhibited a high sensitivity of 1.28×10^6 kPa^{-1} and a wide sensing range of 4.51–54,837.06 Pa. Furthermore, single-walled carbon nanotubes (SWCNTs) were introduced into the micropyramid arrays. SWCNTs blended with the elastomer pyramids dramatically improved the adhesion between the conductive Au layer and the elastomer micropyramids and created new conductive paths that could enhance the sensor sensitivity. As a result, the hysteresis of the sensor was greatly reduced (~2.52%). In addition, good cycling stability of the sensor was achieved with no performance decrease after 2000 cycles of pressure. Furthermore, the pressure mapping was successfully achieved using a 3 × 3 sensor array. Finally, as a proof of concept, the sensor was employed to detect a series of pressure signals, including pulse, speech, and swallowing, which can be potentially used to prevent diseases such as amyotrophic lateral sclerosis (ALS) and cardiovascular disease. In addition, the sensor enabled the manipulator to imitate human gestures, as well as grasp and identify objects of various masses. These results demonstrate that our sensors with high sensitivity, low hysteresis, and a wide detection range exhibit great potential in healthcare and artificial intelligence.

2. Experimental section

2.1. Reagents and instruments

The details of the instruments and reagents used in this experiment can be found in the SI.

2.2. Fabrication of a flexible piezoresistive sensor

The steps for fabricating a silicon template were as follows. First, the silicon wafer was cleaned by sonicating in each of acetone, ethanol, and deionized water for 15 min before being dried under a stream of N_2. Next, the mask pattern was fabricated on the surface of the pre-processed silicon wafer using photolithography. To remove the SiO_2 layer that was not protected by the photoresist, the silicon wafer was treated with a buffered oxide etchant solution (NH_4F:HF = 7:1, v/v). Finally, the patterned silicon wafer was anisotropically etched in a potassium hydroxide (KOH) (35 wt%) and isopropanol solution (KOH:isopropanol = 5:1, v/v) at 80 ˚C under vigorous stirring. Subsequently, a buffered oxide etchant solution was used to remove the remaining SiO_2 layer, resulting in a silicon template with MADHs. Notably, the silicon template could be reused, allowing the MADH sensor to be manufactured on a large scale.

Preparation of silicon templates for hydrophobization: The following surface treatment activities were performed to ensure that the produced sensor film could be easily transferred from the MADH template. The surface of the template was first treated with plasma in an O_2 environment for 3 min (30 W, CPC-A, CIF International Group Co., Ltd). The template surface was then fluorinated using 1H, 1H, 2H, 2H-perfluorooctyltrimethoxysilane steam (200 ˚C, 3 h). Finally, a hydrophobized MADH silicon template was obtained.

Preparation of the MADH conductive film: Under agitation, SWCNTs (conductive material) were dispersed in PDMS (elastomer) to form a homogeneous solution. To obtain the SWCNT/PDMS elastomer film, a certain amount of curing agent was added (the ratio of precursor to curing agent was 10:1, w/w) and the solution was spin-coated on the pretreated silicon template. The solution was then vacuum degassed to eliminate interference from bubbles in the solution. To achieve a MADH SWCNT/PDMS film, the solution was dried for 3 h at 90 ˚C and the conductive elastomer (9.47 S cm^{-1}, **Figure S3, SI**) was peeled away from the silicon template. Finally, to form a double-layer conductive film (Au/SWCNT/PDMS), an Au film (80 nm) was deposited on the surface of the SWCNT/PDMS elastomer.

Fabrication of MADH flexible piezoresistive sensors: First, to eliminate surface contaminants, a polyethylene terephthalate (PET) membrane (0.5 mm thick) was sonicated for 15 min sequentially with acetone, ethanol, and water. Then, using thermal evaporation, a conductive material (Cr/Au, 10/60 nm) was deposited on the surface of PET to form interdigital electrodes. Finally, the MADH film was assembled on the PET interdigital electrodes to fabricate a tactile sensor.

2.3. Finite Element Analysis (FEA) simulation method

The deformation of the pyramid membrane during the stress process was simulated using ABAQUS FEA software. The elastic modulus of the interdigital electrode is much larger compared to that of the pyramidal microstructure. Therefore, the interdigital electrode is simplified to a rigid body model, and it is held stationary during the simulation. The pyramid membrane model was modeled using the Mooney–Rivlin hyperelastic model, and the simulation parameters are shown in **Table S1 (SI)**. To save computing resources, we simplified the MADH membrane into a 3×3 array and modeled it using 3D model with the size of the actual microstructure. The detailed number of elements or nodes is shown in **Table S2 (SI)**. Tetrahedral elements (C3D4) were used to mesh the model. The boundary condition imposed on the model is the pressure, and the constraint makes it move only in the direction of the pressure. Different pressures were applied to the upper surface of the membrane in the vertical direction, and the variations in the rate of change in the contact area and the displacement were recorded. The initial area of different models is obtained under the same applied pressure condition (**Table S3, SI**). All computation is conducted on a computer of Intel(R) Core(TM) i7-11800H CPU&16G RAM.

3. Results and discussion

3.1. Preparation principle and preparation process of the MADH tactile sensor

For piezoresistive pressure sensors, the sensor sensitivity is represented by the rate at which the contact area of the conductive path changes, as a high contact area change rate contributes to a considerable change in the resistance of the sensor. Furthermore, the contacting state of the conductive path under different pressures can predict the pressure-detection range of the sensor. Therefore, for the rational design of a pressure sensor with high sensitivity and a wide pressure detection range, the rate of change in the contact area between the active electrode with micropyramid arrays and the flat current collecting electrode was analyzed using simulation (**Figure S4, SI**). The contact area change rate increased when the density of the micropyramid decreased, demonstrating that a higher sensitivity of the sensor could be realized.

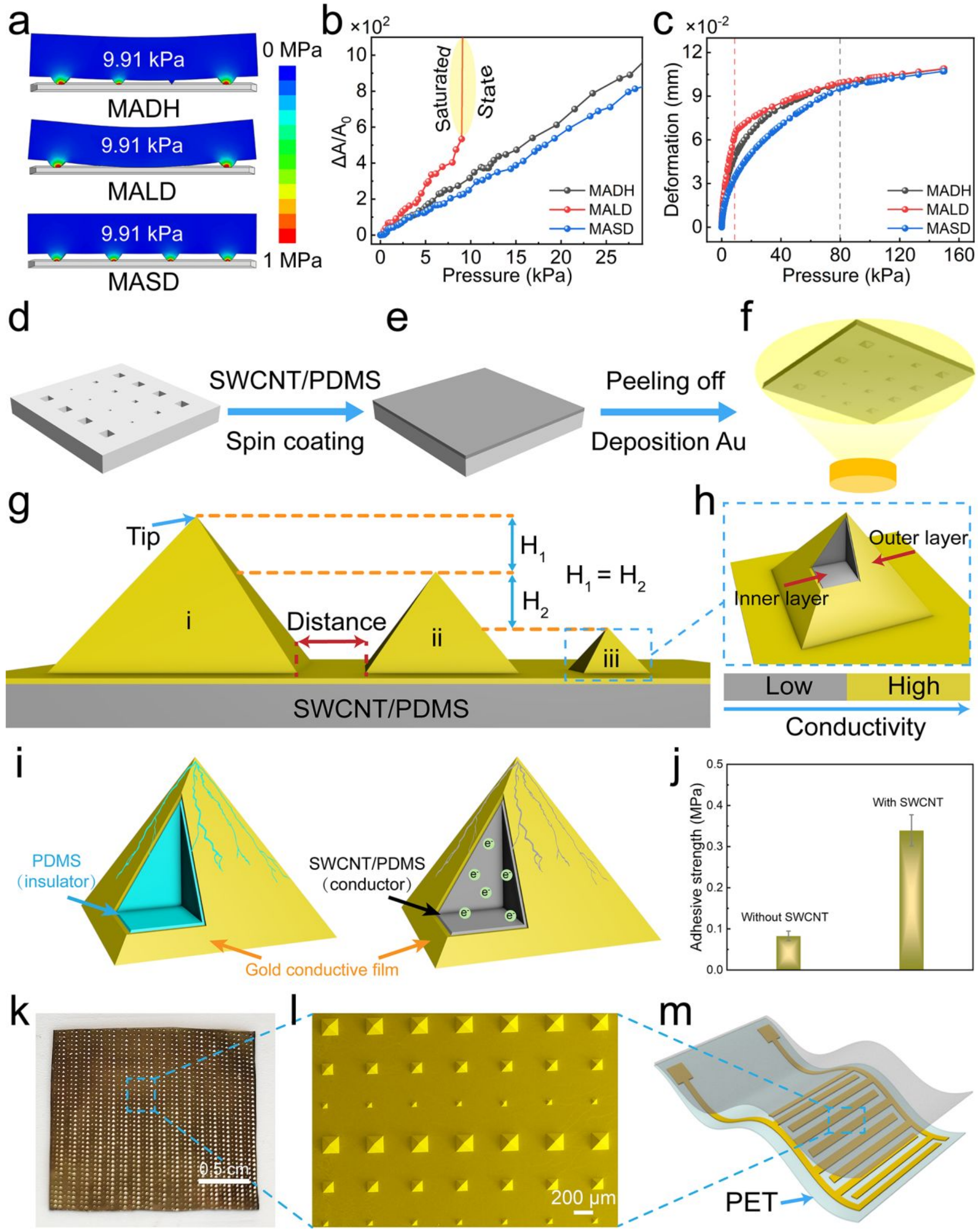

Figure 1. (a) Stress distributions of the micropyramid arrays with different morphologies under pressing, and their (b) contact area change rates and (c) deformation (deformation is the average

vertical displacement of the top surface) obtained using the finite element analysis (FEA). (d–f) Schematic diagram of MADH sensor preparation. (g) Schematic illustration of the SWCNT/PDMS MADH structure. (h) Schematic diagram of the two conductive paths of MADH. (i) Schematic diagram of the random cracks generated on the Au film under applied pressure. Among them, the SWCNT/PDMS material (right one) can compensate for the conductivity decrease caused by Au film cracks. (j) Adhesion strength between a PDMS film (with and without SWCNTs) and an Au film, error bar, SD (±0.025), n = 5. (k) Photograph of the Au/SWCNT/PDMS MADH film. (l) SEM image of MADH (the gold color was added to the SEM image using Photoshop software). (m) Schematic diagram of the MADH tactile sensor.

However, after decreasing the density of the micropyramids, the contact area between the micropyramid and the flat current collecting electrode became saturated under a relatively low pressure, limiting the pressure-detection range of the sensor. Herein, we assumed that the MADH sensor could achieve the goals of a high contact area change rate and a large pressure response range. As shown in **Figures 1a** and **1b**, the contact area change rate of the MADH was comparable to that of the micropyramid array with low density (Abbreviated as MALD) (**Movies S1** and **S2**) (the density is defined as the number of micropyramids in a unit area). Furthermore, the MADH maintained a high-pressure response, which was larger than that of the micropyramid array with low density but similar to that of the micropyramid array with the same density (Abbreviated as MASD) (**Figure 1c** and **Movie S3**). In this design, the density of the micropyramid with the largest dimensions was low, resulting in a high contact area change rate during the initial pressing state, which represents a high sensitivity. Subsequently, even under higher pressures, the contact area of the micropyramids with smaller dimensions continued to change; hence, the pressure sensing range was enlarged. Therefore, the MADH was expected to provide the tactile sensor with both high sensitivity and a wide pressure detection range. To fabricate the proposed MADH, a silicon template was first fabricated. Then, a conductive elastomer precursor was spin-coated onto the silicon template and peeled off after curing (**Figures 1d–1f** and **S5, SI**). The silicon template was fabricated using photolithography and the alkaline wet etching technology.[30-31] Micropyramid arrays with different densities and heights were prepared by adjusting the size of the inverse-pyramid groove in the silicon template. The conductive elastomer precursor was prepared by blending the SWCNT conductive materials into the PDMS precursors (obtained by homogeneously dispersing 10% SWCNTs in a 90% vinyl terminated PDMS precursor) (**Figure S3, SI**). The Raman spectrum (**Figure S6, SI)** shows that the SWCNTs were dispersed homogeneously in PDMS. Finally, Au was deposited on the surface of the conductive elastomer film (Au/SWCNT/PDMS). More details can be found in the Experimental section.

Figure 1g schematically depicts the MADH structure. In this work, the height difference (ΔH_x) and the edge-to-edge distance between the two neighboring pyramids (D_x) (“x” represents the exact value of the height difference and distance (μm), respectively) were adjusted to optimize the performance of the tactile sensors. **Figure 1h** schematically illustrates the micropyramid structure with two conductive paths. One conductive path is provided by the SWCNTs embedded in the elastomer and the other path is provided by the Au film on the pyramid surface. Although the Au film has good conductivity, which can improve the sensitivity of the sensor, it inevitably forms random cracks as the applied pressure increases.[23] Such random cracks always cause a sudden rise in resistance, adversely affecting the sensitivity of the sensor. Notably, the conductive path provided by the SWCNTs can effectively compensate for the decrease in conductivity, which enhances the sensitivity of the sensor over a wide detection range (**Figure 1i**).

Furthermore, the adhesion strength of Au to the SWCNT/PDMS film was ~4.2 times greater than that of Au to the unmodified PDMS film (**Figure 1j**) (the adhesion strength measurement method is schematically shown in **Figure S7, SI**). This is attributable to the numerous hydroxyl groups on the SWCNT walls, which reduced the surface energy of the elastomer (as demonstrated by the contact angle in **Figure S8, SI**) and enhanced the Au film adhesion.[32-33] Au/SWCNT/PDMS film photographs (**Figures 1k and Figure S8c**) and scanning electron microscopy (SEM) images (**Figure 1l**) show that the MADH was successfully prepared (more micropyramid arrays with different heights and distances are shown in **Figure S9, SI**). Subsequently, the tactile sensor was prepared by assembling the MADH on the interdigital Au electrodes, which were deposited on the flexible PET substrates (**Figure 1m**) (more details of the tactile sensor fabrication process can be found in the Experimental section).

3.2. Working mechanism, sensitivity and simulation analysis of the MADH tactile sensor

The working mechanism of the tactile sensor is displayed in **Figure 2a**. As the pressure increased, the contact area between the MADH and the interdigital electrodes increased, causing a decline in contact resistance. Moreover, owing to deformation of MADH film causing by the pressure, the distance between the conductive agents within the SWCNT/PDMS conductive film is reduced to quantum size (tunnelling effect)[34-35] or contact (percolation effect).[36-40] As a result, the sensor is able to form more conductive pathways (**Figures 2b and S10**). Accordingly, under the synactic effects (**Figures S10 and S14, SI**) of the contact area change rate, percolation effect, and tunneling effect, the current of the MADH sensor increased with increasing pressure. The sensitivity of the sensor was investigated and optimized at 25 ℃ by employing MADHs with different micropyramid densities as the active electrode. The micropyramid arrays with the same height difference (ΔH = 30 μm (ΔH_{30})) were separated by different distances (D = 80, 180, 280, and 380 μm) (**Figure S9, SI**). The sensitivity was calculated using equation 1:

$$S = (\Delta I/I_0)/\Delta P \qquad (1)$$

where ΔI denotes the relative change in current, I_0 is the initial current without pressure, and P is the applied pressure. The sensitivity increased from 8.61×10^5 to 1.40×10^6 kPa^{-1} with the decrease in the micropyramid density (**Figures 2c** and **2d**). The change in the sensitivity was also evidenced using the FEA simulation results (**Figure 2e**). The simulated sensitivity of the sensor was represented by the area change rate of the micropyramid arrays, as calculated using equation 2:

$$\text{Area change rate} = (A - A_0)/A_0 = \Delta A/A_0 \qquad (2)$$

where A_0 and A represent the initial contact area and the contact area under pressure, respectively. The increased sensitivity was attributed to the higher stress concentration at the tips of the low-density micropyramids.

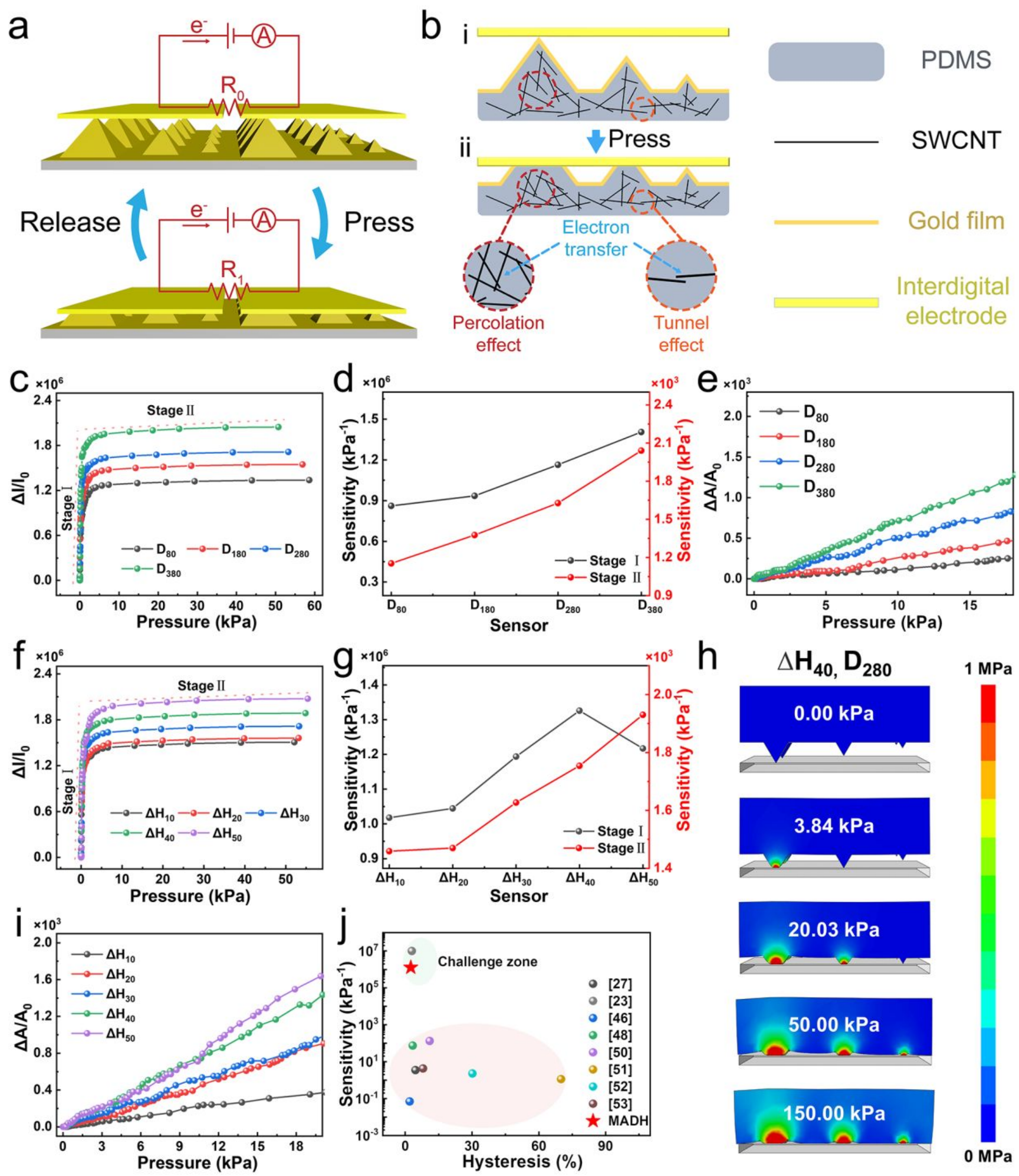

Figure 2. (a) Schematic description of the working mechanism of the MADH sensor under an applied pressure (R_0 and R_1 represent the initial resistance and the resistance after applying pressure, respectively). (b) Schematic diagram of the percolation effect and tunneling effect of the SWCNT/PDMS sensor under pressure. (c and d) Relative current response of the sensors (with

different pyramid distances) under different pressures and their corresponding sensitivities (under 1 V constant voltage condition). (e) FEA simulations of the contact area change rate of MADHs (with different pyramid distances (D_x)) under different pressures. (f and g) Relative current responses of sensors (with different pyramid heights (ΔH_x)) under different pressures and their corresponding sensitivities. (h) Stress distribution of the MADH (ΔH_{40}, D_{280}) acquired using FEA with an increase in applied pressure. (i) FEA simulation results of the contact area change rate of MADHs (with different pyramid heights (ΔH_x)) under pressure. (j) Sensitivity comparison of our MADH sensor with other published flexible piezoresistive sensors.

However, compared with the high-density micropyramids (D_{80}), the low-density micropyramids (D_{380}) caused saturation of the contact area between the pyramids and the electrode substrate at a lower pressure (**Figures S11 and S12**), reducing the detection range of the sensor. Hence, although D_{380} showed a relatively high sensitivity, it more easily reached saturation at a low pressure. In this study, we chose the micropyramid arrays with 280 μm distances (D_{280}) between each pyramid for the fabrication of tactile sensors with high sensitivity and a wide pressure detection range.

Consequently, to further address the trade-off between the high sensitivity and wide pressure detection range, we adjusted the height difference (ΔH_x, x = 10, 20, 30, 40, and 50 μm) of the pyramid arrays while maintaining the same distance (D_{280}) (**Figure S9, SI**). As shown in **Figures 2f** and **2g**, the sensitivity increased as the height difference increased from ΔH_{10} to ΔH_{40}. This occurred because as the height difference increased, more stress was concentrated at the tips of the largest micropyramids. As a result, a high contact area change rate was achieved, and thus the sensitivity effectively increased. Notably, the sensitivity of the ΔH_{50} MADH sensor was lower than those of the other sensors (ΔH_{10}, ΔH_{20}, ΔH_{30}, and ΔH_{40}) at lower pressures. This occurred because as the height difference increased from ΔH_{10} to ΔH_{50}, the dimensions of the largest pyramid in the MADH grew continuously, resulting in a larger pressure required to compress the pyramids with large dimensions. This leads to a decrease in the sensitivity of the ΔH_{50} sensor in the sensing range under low pressures (from 7.06 to 1922.54 Pa). In the higher-pressure range (>2148.18 Pa), the sensitivity of the sensors increased with the increase in the height difference of the micropyramid arrays. This possibly occurred because, after the micropyramids with lower heights were compressed, the total contact area change rates were larger in the ΔH_{50} micropyramid arrays than in the other micropyramid arrays (ΔH_{10}, ΔH_{20}, ΔH_{30}, and ΔH_{40}) because it was much easier to compress the micropyramids when the stress was just starting to concentrate at the tips. This trend was also evidenced in the simulation result (**Figure 2i**). The process of stress increasing with pressure during the simulation is shown in **Figures 2h** and **S13 (SI)** and **Movie S4**. The area change rate of the ΔH_{10}, ΔH_{20}, ΔH_{30}, and ΔH_{40} micropyramid arrays increased gradually with the increase in pressure. Although the area change rate of the ΔH_{50} micropyramid arrays was reduced at low pressures, it gradually surpassed the area change rate of the ΔH_{40} micropyramid arrays at high pressures. Thus, sensors fabricated from the ΔH_{50} micropyramid arrays showed a relatively low sensitivity in the low-pressure range. We selected the sensors based on micropyramid arrays with parameters ΔH_{40} and D_{280} for the following investigation because they possessed the highest sensitivity (1.28×10^6 kPa^{-1}), which is quite important for electronic skin,[41-42] and they maintained a wide pressure detection range (4.51–54837.06 Pa). Notably, the sensitivity of the MADH tactile sensors was higher than that of most flexible pressure sensors with a microstructure design (**Figure 2j** and **Table S4, SI**).[27, 43-45]

Another important parameter for tactile sensors is hysteresis, which represents the difference in pressure signal transmission after pressure loading and unloading. A low hysteresis of the sensor is important for accurate sensing of the pressure.[46-47] Currently, the main cause of high hysteresis is external energy losses during material compression.[48-49] These losses are a result of (i) energy consumption caused by friction/adhesion during contact between sensing materials and electrodes, particularly for elastomer materials, and (ii) the sensor continuously consumes energy during the deformation process because of the weak interactions between the conductive material and the elastomer. To address these issues, we deposited an Au conductive film on the SWCNT/PDMS elastomer surface to realize a bimetallic electrode interface. This can effectively suppress the energy losses caused by friction/adhesion resulting from the direct contact between the conductive elastomer and the interdigital metal (Au) electrodes. Furthermore, the SWCNTs mixed in the elastomer compensated for the resistance change caused by random cracks in the Au film. More importantly, the SWCNTs increased the adhesion of the Au film to the elastomer, which was expected to reduce energy losses caused by friction. Hence, the hysteresis of the as-prepared tactile sensor based on MADH (Au/SWCNT/PDMS) was reduced to ~2.52%, which was lower than those of the SWCNT/PDMS (~7.31%) and Au/PDMS (~5.30%) sensors (**Figure S14, SI**). The process for calculating hysteresis is shown in **Figure S15 (SI**). We compared the sensitivity and hysteresis of the MADH sensor with those of the published works. As shown in **Figure 2j**, our sensor exhibited better sensitivity and hysteresis (**Table S5, SI**) compared to other flexible tactile sensors.[23, 27, 46, 48, 50-53] Hence, we provide a reference strategy for fabricating tactile sensors with high sensitivity and low hysteresis.

3.3. Characterization of the sensing performance of the MADH tactile sensor

In practical applications, stability and fast response are also important parameters for tactile sensors. The stable sensing performance of our MADH tactile sensor was achieved by repeatedly loading and unloading the same pressure (1074.5 Pa) on the sensor (**Figures 3a** and **3b**). In addition, we monitored the MADH sensor under various pressures. As shown in **Figure 3c**, the sensor responded quickly and consistently, indicating its good stability. The sensor maintained a strong linear relationship (this includes two linear sensing stages (4.51–1400.78 Pa and 7180.25–54837.06 Pa)) and a stable response behavior (**Figure 3d**). In addition, we connected a LED with a "HIT" pattern in series with the MADH sensor (**Figure 3e**). The brightness of the LED light increased with the increase in applied pressure under a constant voltage (10 V). These results show that a good ohmic contact was formed between the MADH sensing material and the interdigital electrodes.[54] Furthermore, the response behavior of the MADH sensor was monitored under a constant pressure at various frequencies (**Figure 3f**). The results show that the sensor always responded quickly and stably without delay, indicating that the sensor had good repeatability, as well as a quick response (0.149 s) and recovery time (0.138 s) (**Figures 3g and S16**).

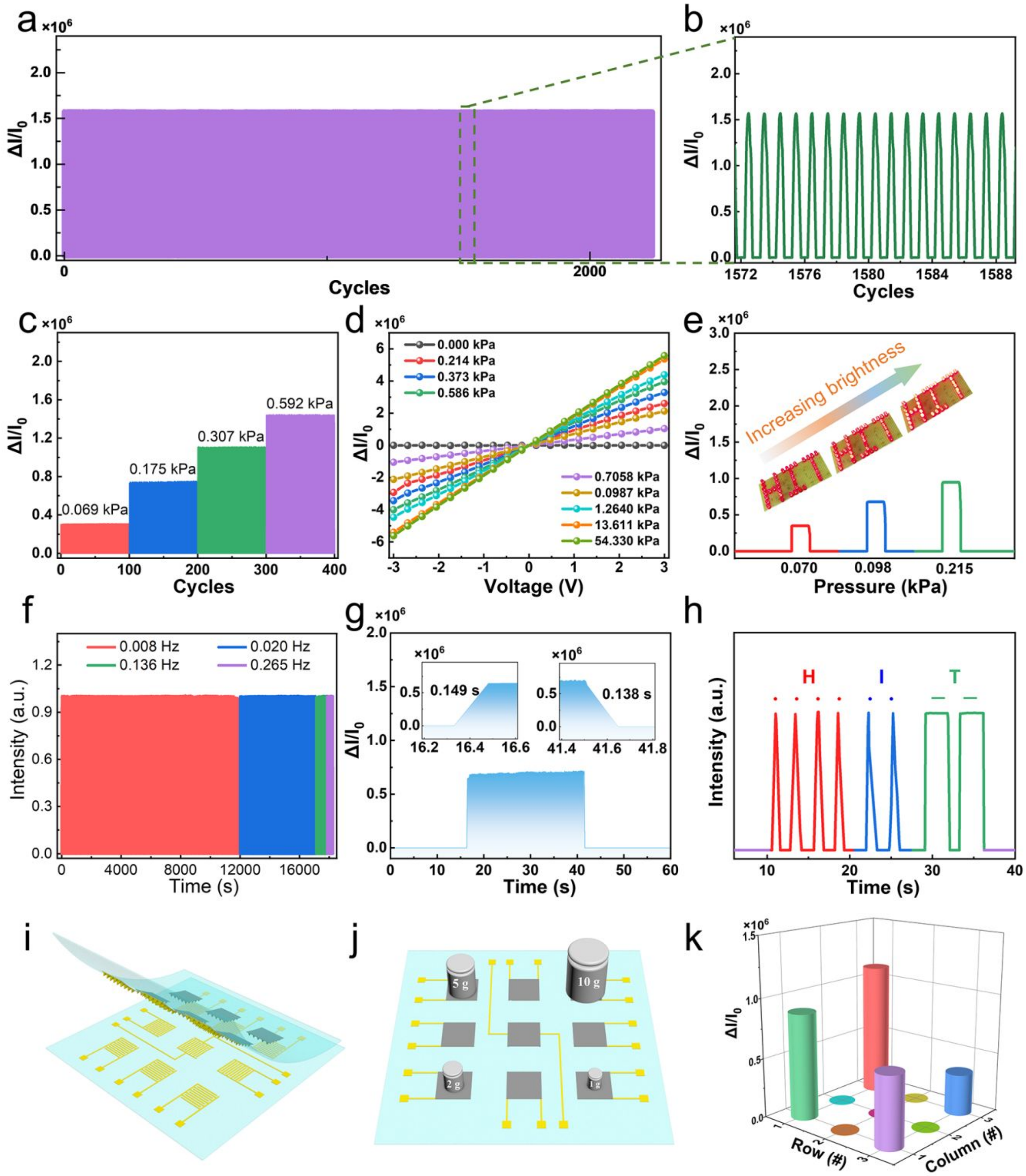

Figure 3. (a and b) Durability of the MADH sensor over 2000 cycles of pressure loading/unloading. (c) Relative current response of the MADH sensor under different pressures. (d) Current–voltage curves of the MADH sensor with increasing pressure. (e) Illumination of the LED array (connected

by the sensors) after increasing the pressure applied to the sensors. (f) The response of the MADH sensor under the same pressure at different frequencies. (g) The response of the sensor under a loading/unloading pressure of 0.10 kPa. The inset is an enlarged picture of the response and relaxation time. (h) Morse code diagram of "HIT". (i) Schematic diagram of the sensor array, (j) schematic drawing of four objects with different weights placed on the sensor array, and (k) the response of the sensor array.

In addition, Morse code could be defined using the duration and frequency of the response of the MADH sensor (**Figure 3h**). We encoded a Morse code according to the duration and frequency of finger bending, and the results showed that the "HIT" Morse code was successfully demonstrated. To verify the sensing ability of the sensor in the spatial pressure distribution, the MADHs were assembled into a 3 × 3 array (**Figures 3i** and **3j**). Simultaneously, in order to better identify the weight of heavy objects, we have calibrated every single sensor of the sensor array before testing the performance of the array (**Figure S17, SI**). As shown in **Figure 3k**, the device accurately identified the weights and positions of various objects.

3.4. Application of the MADH tactile sensor in health monitoring

Moreover, the MADH tactile sensor has great potential in wearable bioelectronics to monitor human activities and subtle physiological signals in real time. For wearable electronics, low energy consumption is a basic requirement to reduce the dimensions and weight of the power source and prolong the working time of the system. As shown in **Figure 4a**, the sensor quickly responded to finger pressing with different pressures. Notably, when the pressure was removed, the current response of the sensor disappeared instantaneously, indicating that the device consumed less power while in standby mode. When the sensor was worn on human skin, it successfully detected joint movements of the human body. The pressure generated by the bending of the wrist (**Figure 4b**), knee (**Figure S18a, SI**), or finger (**Figure 4c**) was successfully detected, which can be used to measure the health status during rehabilitation.[55-56]

The sensor can be used for medical health monitoring. Amyotrophic lateral sclerosis (ALS) is a progressive degenerative neurological disease affecting motor neurons. In the early stage, ALS patients not only have difficulty chewing, walking, swallowing, and speaking, etc., but also suffer from muscle atrophy in the extremities (e.g., legs). In the later stage, they may completely lose motor function.[57] In such cases, the patient must be able to communicate with his/her surroundings and receive rehabilitation training.[58] Notably, the MADH soft tactile sensor can be flexibly attached to the corner of the eye, masseter muscle (face), and throat using medical tape (shown in **Figures 4d** and **4e** inset) to detect small deformations of the skin. Simultaneously, the MADH sensor could clearly distinguish the frequency and intensity of blinking (**Figure 4d**) and masseter muscle movements (**Figure 4e**). In addition, the relative response of the MADH sensor to swallowing (**Figure S18b, SI**) can be used to assess the state of ALS under different conditions and provide health services for disease prevention.[59-60] Besides which, we used sensors to monitor different gaits (the sensor is placed on the heel of the foot). It turns out that the sensor can distinguish the motion state (e.g., standing and running) based on the waveform, frequency and intensity of the signal (**Figure S18c**). This means that the gait signals monitored by the sensors can be used to assess the physical health of ALS patients during the rehabilitation process. The MADH sensors could distinguish different words (e.g., article and possible) based on the neck muscle movements and vocal cord vibrations of the speaker (**Figure 4f**), demonstrating that MADH sensors have a lot of potential for intelligent speech recognition. Moreover, because of its high sensitivity and low hysteresis, the sensor successfully monitored the subtle physiological signals (pulse) used to identify hypertension, atherosclerosis, and a variety of other cardiovascular diseases.

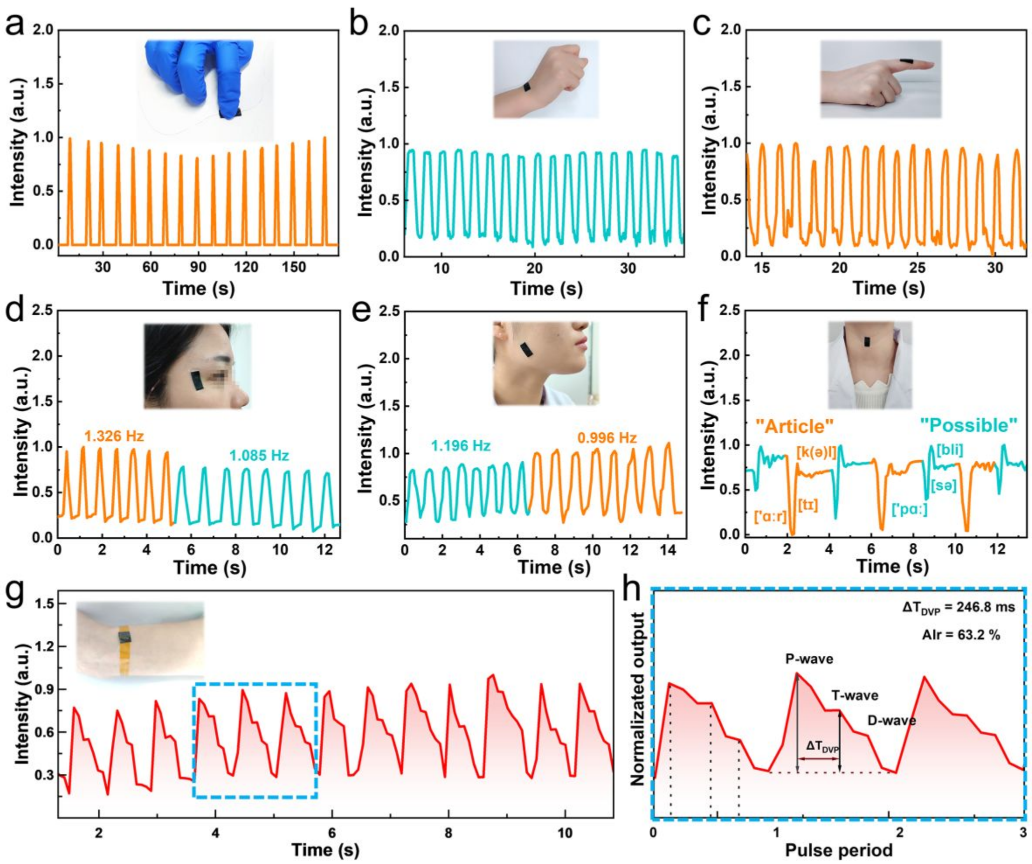

Figure 4. Normalized current responses of the sensor from (a) finger pressing, (b) wrist bending (monitoring at ~45˚ bend), and (c) finger bending (monitoring at ~90˚ bend). (d) Real-time response of the sensor to blinking, (e) vibration of masseter muscle on the face when speaking, and (f) throat vibration when speaking the words "article" and "possibility". (g) Pulse monitoring and (h) the amplified normalized pulse periodic waveform. The inset shows a photograph of the pulse being monitored.

In this study, the MADH sensor was installed on the radial artery of the wrist of a volunteer to monitor the pulse peak (**Figure 4g** and **Movie S5, SI**). A series of rhythmic and steady signals were recorded, showing a normal pulse rate of 83 beats/min. Typical pulse waveforms, such as percussion (P), tidal (T), and diastolic (D) waves, are clearly identified in the enlarged graph. Subsequently, a great deal of useful physiological information was extracted (**Figure 4h**). For example, the time between P and D waves (ΔT_{DVP}) was 246.8 ms, and the radial augmentation index (AIr), which represents the arterial stiffness, was 0.63. The process for calculating the AIr is shown in **Figure S19 (SI)**.[61] The AIr value of 0.63 was within the typical range of 0.5–1.3 (a higher AIr value indicates a higher risk of cardiovascular disease), depicting the healthy cardiovascular system state of the volunteer.[13, 62-63] These findings imply that the MADH tactile sensor with high sensitivity and low hysteresis not only helps to reduce the distortion of the pulse waveform but also can accurately monitor subtle dynamic movement of the human body (e.g., intraocular pressure, gentle touch and respiration, < 1 kPa).[27, 35, 64]

3.5. Application of the MADH tactile sensor in human–machine interaction

The MADH tactile sensor was successful in monitoring both large and subtle motions of the human body, indicating that the sensor had superior capabilities in the field of human–machine interaction. For instance, the smart glove converted the pressure generated by the movement of the finger joints into electrical signals and transmitted them to the controller, which controlled the manipulator to perform the corresponding actions (**Figure S20, SI**).

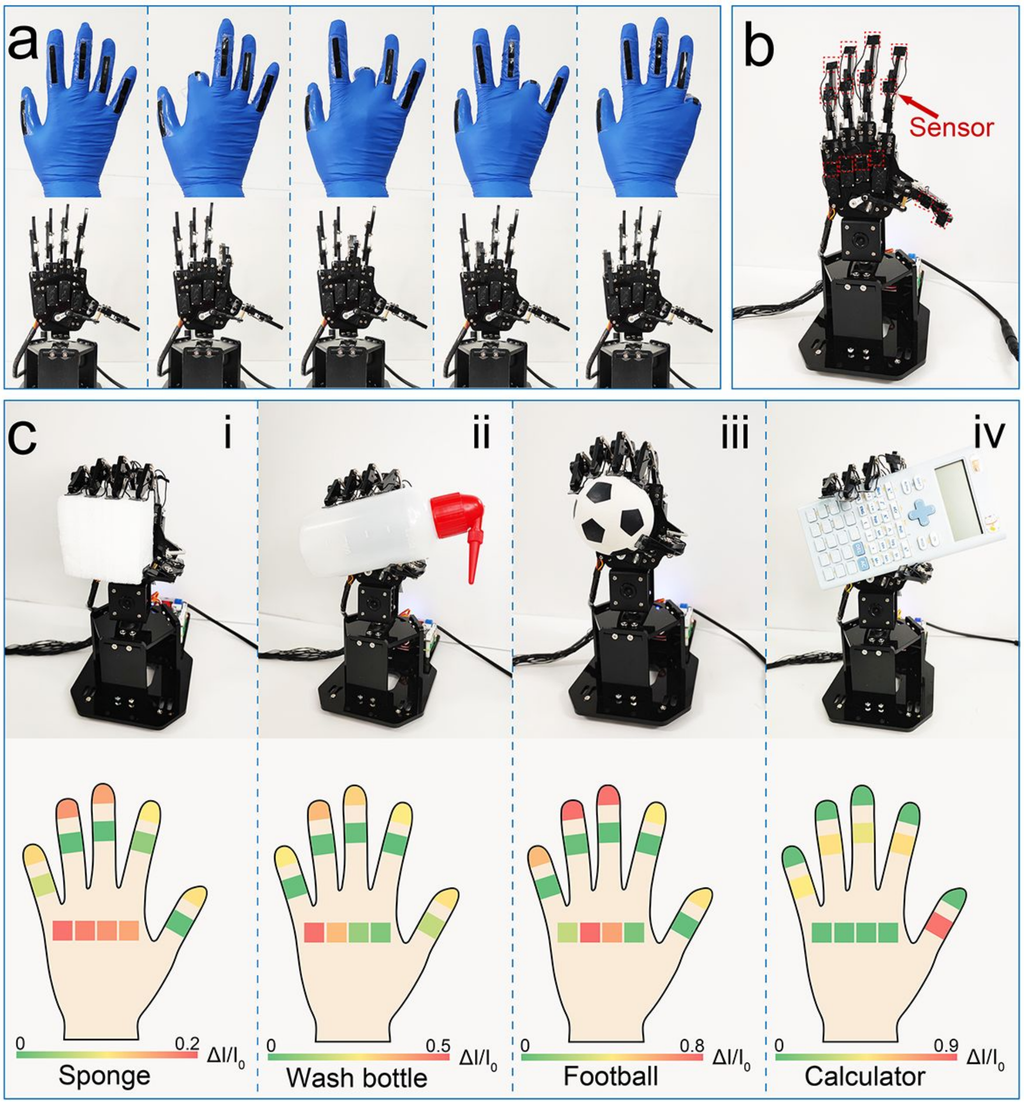

Figure 5. (a) Application of the gesture remote control using the MADH tactile sensors. (b) Image of sensors attached to a robotic hand. (c) Photographs of the manipulator attached to MADH tactile

sensors gripping different objects, and schematic diagrams of the pressure monitored at the positions where the sensors were attached to the manipulator.

As illustrated in **Figure 5a**, when the fingers made specific gestures, the manipulator could imitate the finger movement in real time (**Movie S6**). Simultaneously, when the fingers maintained a gesture, the manipulator followed that gesture, indicating that the soft tactile sensor could respond rapidly and transmit signals reliably.

Moreover, a major application of the tactile sensor is as an electronic skin to enable tactile perception in robots. In this work, we assembled the prepared sensors at the finger joints of a robotic hand (**Figure 5b**). As shown in **Figure 5c**, the manipulator with sensors could grasp objects of various shapes (e.g., sponge (3.18 g), water bottle (33.84 g), soccer ball (53.51 g), and calculator (86.72 g)) (**Figure 5ci–5civ**). For example, when the manipulator was controlled to grasp the calculator, the sensor in the thumb (proximal phalanx), index finger (middle phalanx), middle finger (middle phalanx), ring finger (middle phalanx), and little finger (middle phalanx) responded and exhibited varying degrees of response, whereas the sensors at the other sites did not respond (**Figure 5civ**). Therefore, when the manipulator grasped objects of different shapes, it generated corresponding signals according to the different objects. This indicates that the manipulator with the MADH sensor had good grasping ability and can be expected to recognize objects of different shapes.

4. Conclusions

In summary, we created a piezoresistive tactile sensor based on a MADH. The MADH regulated the strain distribution on the active electrode of the tactile sensor, providing the sensor with both high sensitivity (1.28×10^6 kPa^{-1}) and a large pressure detection range (4.51–54837.06 Pa). To make the MADH conductive, we incorporated SWCNTs into the micropyramid array and deposited an Au film on its surface. The SWCNTs formed a conductive path inside the elastomer micropyramids owing to the percolation effect and the tunneling effect, which can compensate for resistance changes caused by random cracks in the Au film. Hence, the high sensitivity of the sensor was realized. Moreover, the SWCNTs increased the adhesion strength between the Au film and the elastomer, which plays a key role in reducing the hysteresis of the MADH sensor, and hysteresis as low as ~2.52% was achieved. Our sensor exhibited much better sensitivity and lower hysteresis (**Table S5, SI**) than most of the reported flexible tactile sensors. Finally, the sensor was successfully applied to real-time monitoring of human activities (e.g., pronunciation, swallowing, and chewing) and subtle physiological signals (e.g., pulse). Moreover, the sensors could be used to control the movement of the manipulator as well as to enable the manipulator to grasp different objects. Therefore, our work provides an effective strategy to address the trade-off between high sensitivity and a large detection range of the flexible tactile sensor. Moreover, this work paves the way to reduce hysteresis in flexible tactile sensors.

ASSOCIATED CONTENT

Supporting Information

Comparison graph of sensitivity and detection range of published literature; preparation diagram of sensor; Photo of the prepared electrode; finite element simulations, Raman, SEM, SWCNT/PDMS conductivity, contact angle and hysteresis data; schematic diagram of the adhesion strength and hysteresis calculation data; schematic diagram of the equivalent circuit and sensor remote manipulator; health monitoring data for foot gait, knee flexion and swallowing; Comparison table of sensor performance (PDF)

Under compression, a finite element analysis of micro-pyramid arrays of different heights (ΔH_{30}, D_{280}) is performed (MP4)

Under compression, a finite element analysis of the micro-pyramid array with low density is performed (MP4)

Under compression, a finite element analysis of pyramid array with the same density is performed (MP4)

Under compression, a finite element analysis of micro-pyramid arrays with different heights (ΔH_{40}, D_{280}) is performed (MP4)

Pulse monitoring in real time using a soft tactile sensor (MP4)

Flexible tactile sensors are used in a real-time human-machine interaction system (MP4)

AUTHOR INFORMATION

Corresponding Author

Dianpeng Qi - National and Local Joint Engineering Laboratory for Synthesis, Transformation and Separation of Extreme Environmental Nutrients; MIIT Key Laboratory of Critical Materials Technology for New Energy Conversion and Storage, School of Chemistry and Chemical Engineering, Harbin Institute of Technology, Harbin 150001, P. R. China. Email: dpqi@hit.edu.cn

Yan Liu - National and Local Joint Engineering Laboratory for Synthesis, Transformation and Separation of Extreme Environmental Nutrients; MIIT Key Laboratory of Critical Materials Technology for New Energy Conversion and Storage, School of Chemistry and Chemical

Engineering, Harbin Institute of Technology, Harbin 150001, P. R. China. Email: liuyan1986@hit.edu.cn

Authors

Cuiyuan Liang - National and Local Joint Engineering Laboratory for Synthesis, Transformation and Separation of Extreme Environmental Nutrients; MIIT Key Laboratory of Critical Materials Technology for New Energy Conversion and Storage, School of Chemistry and Chemical Engineering, Harbin Institute of Technology, Harbin 150001, P. R. China.

Jingqi Sun - National and Local Joint Engineering Laboratory for Synthesis, Transformation and Separation of Extreme Environmental Nutrients; MIIT Key Laboratory of Critical Materials Technology for New Energy Conversion and Storage, School of Chemistry and Chemical Engineering, Harbin Institute of Technology, Harbin 150001, P. R. China.

Zhihua Liu - Institute of Materials Research and Engineering, Agency for Science, Technology and Research (A*STAR), 138634, Singapore.

Gongwei Tian - National and Local Joint Engineering Laboratory for Synthesis, Transformation and Separation of Extreme Environmental Nutrients; MIIT Key Laboratory of Critical Materials

Technology for New Energy Conversion and Storage, School of Chemistry and Chemical Engineering, Harbin Institute of Technology, Harbin 150001, P. R. China.

Qinyi Zhao - National and Local Joint Engineering Laboratory for Synthesis, Transformation and Separation of Extreme Environmental Nutrients; MIIT Key Laboratory of Critical Materials Technology for New Energy Conversion and Storage, School of Chemistry and Chemical Engineering, Harbin Institute of Technology, Harbin 150001, P. R. China.

Dan Yang - National and Local Joint Engineering Laboratory for Synthesis, Transformation and Separation of Extreme Environmental Nutrients; MIIT Key Laboratory of Critical Materials Technology for New Energy Conversion and Storage, School of Chemistry and Chemical Engineering, Harbin Institute of Technology, Harbin 150001, P. R. China.

Jianhui Chen - National and Local Joint Engineering Laboratory for Synthesis, Transformation and Separation of Extreme Environmental Nutrients; MIIT Key Laboratory of Critical Materials Technology for New Energy Conversion and Storage, School of Chemistry and Chemical Engineering, Harbin Institute of Technology, Harbin 150001, P. R. China.

Bowen Zhong - National and Local Joint Engineering Laboratory for Synthesis, Transformation and Separation of Extreme Environmental Nutrients; MIIT Key Laboratory of Critical Materials

Technology for New Energy Conversion and Storage, School of Chemistry and Chemical Engineering, Harbin Institute of Technology, Harbin 150001, P. R. China.

Ming Zhu - National and Local Joint Engineering Laboratory for Synthesis, Transformation and Separation of Extreme Environmental Nutrients; MIIT Key Laboratory of Critical Materials Technology for New Energy Conversion and Storage, School of Chemistry and Chemical Engineering, Harbin Institute of Technology, Harbin 150001, P. R. China.

Hongbo Xu - National and Local Joint Engineering Laboratory for Synthesis, Transformation and Separation of Extreme Environmental Nutrients; MIIT Key Laboratory of Critical Materials Technology for New Energy Conversion and Storage, School of Chemistry and Chemical Engineering, Harbin Institute of Technology, Harbin 150001, P. R. China.

Author Contributions

D. Q., Y. L.: Resources, formal analysis, supervision, conceptualization, project management, and funding acquisition. D. Q., Y. L. and C. L.: Conceived the ideas, and designed the experiments. C. L.: Survey, conceptualization, methodology, software, data analysis and wrote the manuscript. With the assistance of J.S., Z.L., G.T., Q.Z., D.Y., J.C., B.Z., M.Z. and H.X., C. L. completed all experiments. The manuscript was written through contributions of all authors. All authors have given approval to the final version of the manuscript.

Notes

The authors declare that they have no conflict of interest.

Acknowledgments

The authors acknowledge funding support from the National Natural Science Foundation of China (Grants No. 52173237 and 51903068), the Natural Science Foundation of Heilongjiang Province, China (YQ2020E001), The Interdisciplinary Research Foundation of HIT (IR2021207), the Project of National Centre for International Research on Intelligent Nano-Materials and Detection Technology in Environmental Protection, Soochow University (No. SDGH2105), and The Open Project Program (PEBM202107) of Key Laboratory for Photonic and Electric Bandgap Materials, Ministry of Education.

ABBREVIATIONS

MALD, micro-pyramid array with low density; MASD, micro-pyramid arrays with the same density; MADH, micro-pyramid array with different heights; PDMS, polydimethylsiloxane; SWCNT, single-walled carbon nanotubes; PET, polyethylene terephthalate.

References

(1) He, F.; You, X.; Wang, W.; Bai, T.; Xue, G.; Ye, M. Recent Progress in Flexible Microstructural Pressure Sensors Toward Human–Machine Interaction and Healthcare Applications. Small Methods 2021, 5, 2001041.

(2) Chen, J.; Zhu, Y.; Chang, X.; Pan, D.; Song, G.; Guo, Z.; Naik, N. Recent Progress in Essential Functions of Soft Electronic Skin. Adv. Funct. Mater. 2021, 31, 2104686.

(3) Zhang, S.; Li, S.; Xia, Z.; Cai, K. A Review of Electronic Skin: Soft Electronics and Sensors for Human Health. *J. Mater. Chem. B* **2020,** 8, 852-862.

(4) Mannsfeld, S. C.; Tee, B. C.; Stoltenberg, R. M.; Chen, C. V.; Barman, S.; Muir, B. V.; Sokolov, A. N.; Reese, C.; Bao, Z. Highly Sensitive Flexible Pressure Sensors with Microstructured Rubber Dielectric Layers. *Nat. Mater.* **2010,** 9, 859-864.

(5) Sharma, S.; Chhetry, A.; Maharjan, P.; Zhang, S.; Shrestha, K.; Sharifuzzaman, M.; Bhatta, T.; Shin, Y.; Kim, D.; Lee, S. Polyaniline-Nanospines Engineered Nanofibrous Membrane Based Piezoresistive Sensor for High-Performance Electronic Skins. *Nano Energy* **2022**, 106970.

(6) Zhang, X.; Li, Z.; Du, W.; Zhao, Y.; Wang, W.; Pang, L.; Chen, L.; Yu, A.; Zhai, J. Self-Powered Triboelectric-Mechanoluminescent Electronic Skin for Detecting and Differentiating Multiple Mechanical Stimuli. *Nano Energy* **2022**, 107115.

(7) Li, J.; Yuan, Z.; Han, X.; Wang, C.; Huo, Z.; Lu, Q.; Xiong, M.; Ma, X.; Gao, W.; Pan, C. Biologically Inspired Stretchable, Multifunctional, and 3D Electronic Skin by Strain Visualization and Triboelectric Pressure Sensing. *Small Science* **2022**, 2100083.

(8) Zhang, W.; Xiao, Y.; Duan, Y.; Li, N.; Wu, L.; Lou, Y.; Wang, H.; Peng, Z. A High-Performance Flexible Pressure Sensor Realized by Overhanging Cobweb-like Structure on a Micropost Array. *ACS Appl. Mater. Interfaces* **2020,** 12, 48938-48947.

(9) Tang, Z.; Jia, S.; Wang, F.; Bian, C.; Chen, Y.; Wang, Y.; Li, B. Highly Stretchable Core–Sheath Fibers via Wet-Spinning for Wearable Strain Sensors. *ACS Appl. Mater. Interfaces* **2018,** 10, 6624-6635.

(10) Tang, Z.-H.; Xue, S.-S.; Li, Y.-Q.; Zhu, Z.-C.; Huang, P.; Fu, S.-Y. One-Step Synthesis of Microdome Patterns for Microstructured Pressure Sensors with Ultra-High Sensing Performance. *ACS Appl. Mater. Interfaces* **2021,** 13, 48009-48019.

(11) Ruth, S. R. A.; Feig, V. R.; Tran, H.; Bao, Z. Microengineering Pressure Sensor Active Layers for Improved Performance. *Adv. Funct. Mater.* **2020,** 30, 2003491.

(12) Xiong, Y.; Shen, Y.; Tian, L.; Hu, Y.; Zhu, P.; Sun, R.; Wong, C.-P. A Flexible, Ultra-Highly Sensitive and Stable Capacitive Pressure Sensor with Convex Microarrays for Motion and Health Monitoring. *Nano energy* **2020,** 70, 104436.

(13) Feng, B.; Zou, G.; Wang, W.; Dong, M.; Xiao, Y.; Ren, H.; Zhao, X.; Zhao, G.; Wu, A.; Zhu, H. A Programmable, Gradient-Composition Strategy Producing Synergistic and Ultrahigh Sensitivity Amplification for Flexible Pressure Sensing. *Nano Energy* **2020,** 74, 104847.

(14) Qi, D.; Zhang, K.; Tian, G.; Jiang, B.; Huang, Y. Stretchable Electronics Based on PDMS Substrates. *Adv. Mater.* **2021,** 33, 2003155.

(15) Tian, G.; Yang, D.; Liang, C.; Liu, Y.; Chen, J.; Zhao, Q.; Tang, S.; Huang, J.; Xu, P.; Liu, Z. Non-swelling Hydrogel with Regenerable High Wet Tissue Adhesion for Bioelectronics. *Adv. Mater.* **2023**, 2212302.

(16) Ma, C.; Xu, D.; Huang, Y.-C.; Wang, P.; Huang, J.; Zhou, J.; Liu, W.; Li, S.-T.; Huang, Y.; Duan, X. Robust Flexible Pressure Sensors Made from Conductive Micropyramids for Manipulation Tasks. *ACS Nano* **2020,** 14, 12866-12876.

(17) Huang, Z.; Gao, M.; Yan, Z.; Pan, T.; Khan, S. A.; Zhang, Y.; Zhang, H.; Lin, Y. Pyramid Microstructure with Single Walled Carbon Nanotubes for Flexible and Transparent Micro-Pressure Sensor with Ultra-High Sensitivity. *Sens. Actuators, A* **2017,** 266, 345-351.

(18) Sun, X.; Sun, J.; Zheng, S.; Wang, C.; Tan, W.; Zhang, J.; Liu, C.; Liu, C.; Li, T.; Qi, Z. A Sensitive Piezoresistive Tactile Sensor Combining Two Microstructures. *Nanomaterials* **2019,** 9, 779.

(19) Choong, C.-L.; Shim, M.-B.; Lee, B.-S.; Jeon, S.; Ko, D.-S.; Kang, T.-H.; Bae, J.; Lee, S. H.; Byun, K.-E.; Im, J.; Jeong, Y. J.; Park, C. E.; Park, J.-J.; Chung, U.-I. Highly Stretchable Resistive Pressure Sensors Using a Conductive Elastomeric Composite on a Micropyramid Array. *Adv. Mater.* **2014,** 26, 3451-3458.

(20) Li, H.; Wu, K.; Xu, Z.; Wang, Z.; Meng, Y.; Li, L. Ultrahigh-Sensitivity Piezoresistive Pressure Sensors for Detection of Tiny Pressure. *ACS Appl. Mater. Interfaces* **2018,** 10, 20826-20834.

(21) Zhu, B.; Wang, H.; Liu, Y.; Qi, D.; Liu, Z.; Wang, H.; Yu, J.; Sherburne, M.; Wang, Z.; Chen, X. Skin-Inspired Haptic Memory Arrays with an Electrically Reconfigurable Architecture. *Adv. Mater.* **2016,** 28, 1559-1566.

(22) Yang, J. C.; Kim, J.-O.; Oh, J.; Kwon, S. Y.; Sim, J. Y.; Kim, D. W.; Choi, H. B.; Park, S. Microstructured Porous Pyramid-Based Ultrahigh Sensitive Pressure Sensor Insensitive to Strain and Temperature. *ACS Appl. Mater. Interfaces* **2019,** 11, 19472-19480.

(23) Yao, H.; Yang, W.; Cheng, W.; Tan, Y. J.; See, H. H.; Li, S.; Ali, H. P. A.; Lim, B. Z.; Liu, Z.; Tee, B. C. Near–Hysteresis-Free Soft Tactile Electronic Skins for Wearables and Reliable Machine Learning. *Proc. Natl. Acad. Sci.* **2020,** 117, 25352-25359.

(24) Oh, J.; Kim, J.-O.; Kim, Y.; Choi, H. B.; Yang, J. C.; Lee, S.; Pyatykh, M.; Kim, J.; Sim, J. Y.; Park, S. Highly Uniform and Low Hysteresis Piezoresistive Pressure Sensors Based on Chemical Grafting of Polypyrrole on Elastomer Template with Uniform Pore Size. *Small* **2019,** 15, 1901744.

(25) Chen, J.; Zhang, J.; Luo, Z.; Zhang, J.; Li, L.; Su, Y.; Gao, X.; Li, Y.; Tang, W.; Cao, C.; Liu, Q.; Wang, L.; Li, H. Superelastic, Sensitive, and Low Hysteresis Flexible Strain Sensor Based

on Wave-Patterned Liquid Metal for Human Activity Monitoring. *ACS Appl. Mater. Interfaces* **2020,** 12, 22200-22211.

(26) Zhu, B.; Niu, Z.; Wang, H.; Leow, W. R.; Wang, H.; Li, Y.; Zheng, L.; Wei, J.; Huo, F.; Chen, X. Microstructured Graphene Arrays for Highly Sensitive Flexible Tactile Sensors. *Small* **2014,** 10, 3625-3631.

(27) Zhao, T.; Yuan, L.; Li, T.; Chen, L.; Li, X.; Zhang, J. Pollen-Shaped Hierarchical Structure for Pressure Sensors with High Sensitivity in an Ultrabroad Linear Response Range. *ACS Appl. Mater. Interfaces* **2020,** 12, 55362-55371.

(28) Shi, J.; Lv, S.; Wang, L.; Dai, Z.; Yang, S.; Zhao, L.; Tian, H.; Du, M.; Li, H.; Fang, Y. Crack Control in Biotemplated Gold Films for Wide-Range, Highly Sensitive Strain Sensing. *Adv. Mater. Interfaces* **2019,** 6, 1901223.

(29) Yang, T.; Li, X.; Jiang, X.; Lin, S.; Lao, J.; Shi, J.; Zhen, Z.; Li, Z.; Zhu, H. Structural Engineering of Gold Thin Films with Channel Cracks for Ultrasensitive Strain Sensing. *Mater. Horiz.* **2016,** 3, 248-255.

(30) Qi, D.; Liu, Y.; Liu, Y.; Liu, Z.; Luo, Y.; Xu, H.; Zhou, X.; Zhang, J.; Yang, H.; Wang, W. Polymeric Membranes with Selective Solution-Diffusion for Intercepting Volatile Organic Compounds during Solar-Driven Water Remediation. *Adv. Mater.* **2020,** 32, 2004401.

(31) Qi, D.; Zheng, L.; Cao, X.; Jiang, Y.; Xu, H.; Zhang, Y.; Yang, B.; Sun, Y.; Hng, H. H.; Lu, N. Bio-Inspired Antireflective Hetero-Nanojunctions with Enhanced Photoactivity. *Nanoscale* **2013,** 5, 12383-12387.

(32) Wu, B.; Kuang, Y.; Zhang, X.; Chen, J. Noble Metal Nanoparticles/Carbon Nanotubes Nanohybrids: Synthesis and Applications. *Nano Today* **2011,** 6, 75-90.

(33) Shi, Y.; Wang, Z.; Wen, L.; Pei, S.; Chen, K.; Li, H.; Cheng, H. M.; Li, F. Ultrastable Interfacial Contacts Enabling Unimpeded Charge Transfer and Ion Diffusion in Flexible Lithium-Ion Batteries. *Adv. Sci.* **2022**, 2105419.

(34) Zhong, M.; Zhang, L.; Liu, X.; Zhou, Y.; Zhang, M.; Wang, Y.; Yang, L.; Wei, D. Wide Linear Range and Highly Sensitive Flexible Pressure Sensor Based on Multistage Sensing Process for Health Monitoring and Human-Machine Interfaces. *Chem. Eng. J.* **2021,** 412, 128649.

(35) Shi, L.; Li, Z.; Chen, M.; Qin, Y.; Jiang, Y.; Wu, L. Quantum Effect-Based Flexible and Transparent Pressure Sensors with Ultrahigh Sensitivity and Sensing Density. *Nat. Commun.* **2020,** 11, 3529.

(36) García-Ávila, J.; Rodríguez, C. A.; Vargas-Martínez, A.; Ramírez-Cedillo, E.; Martínez-López, J. I. E-Skin Development and Prototyping Via Soft Tooling and Composites with Silicone Rubber and Carbon Nanotubes. *Materials* **2021,** 15, 256.

(37) Zheng, Y.; Li, Y.; Li, Z.; Wang, Y.; Dai, K.; Zheng, G.; Liu, C.; Shen, C. The Effect of Filler Dimensionality on the Electromechanical Performance of Polydimethylsiloxane Based Conductive Nanocomposites for Flexible Strain Sensors. *Compos. Sci. Technol.* **2017,** 139, 64-73.

(38) Mazumder, S.; Catalan, J. A.; Delgado, A.; Yamaguchi, H.; Villarrubia, C. N.; Mohite, A. D.; Kaul, A. B. Opto-Electro-Mechanical Percolative Composites From 2D Layered Materials: Properties and Applications in Strain Sensing. *Compos. Sci. Technol.* **2019,** 182, 107687.

(39) Zhao, H.; Bai, J. Highly Sensitive Piezo-Resistive Graphite Nanoplatelet–Carbon Nanotube Hybrids/Polydimethylsilicone Composites with Improved Conductive Network Construction. *ACS Appl. Mater. Interfaces* **2015,** 7, 9652-9659.

(40) Yoo, J. Y.; Seo, M. H.; Lee, J. S.; Choi, K. W.; Jo, M. S.; Yoon, J. B. Industrial Grade, Bending-Insensitive, Transparent Nanoforce Touch Sensor Via Enhanced Percolation Effect in a Hierarchical Nanocomposite Film. *Adv. Funct. Mater.* **2018,** 28, 1804721.

(41) Sharma, S.; Chhetry, A.; Maharjan, P.; Zhang, S.; Shrestha, K.; Sharifuzzaman, M.; Bhatta, T.; Shin, Y.; Kim, D.; Lee, S. Polyaniline-Nanospines Engineered Nanofibrous Membrane Based Piezoresistive Sensor for High-Performance Electronic Skins. *Nano Energy* **2022,** 95, 106970.

(42) Wang, X.; Dong, L.; Zhang, H.; Yu, R.; Pan, C.; Wang, Z. L. Recent Progress in Electronic Skin. *Adv. Sci.* **2015,** 2, 1500169.

(43) Wei, Y.; Chen, S.; Lin, Y.; Yang, Z.; Liu, L. Cu–Ag Core–Shell Nanowires for Electronic Skin with a Petal Molded Microstructure. *J. Mater. Chem. C* **2015,** 3, 9594-9602.

(44) Shi, J.; Wang, L.; Dai, Z.; Zhao, L.; Du, M.; Li, H.; Fang, Y. Multiscale Hierarchical Design of a Flexible Piezoresistive Pressure Sensor with High Sensitivity and Wide Linearity Range. *Small* **2018,** 14, 1800819.

(45) Shu, Y.; Tian, H.; Yang, Y.; Li, C.; Cui, Y.; Mi, W.; Li, Y.; Wang, Z.; Deng, N.; Peng, B.; Ren, T.-L. Surface-Modified Piezoresistive Nanocomposite Flexible Pressure Sensors with High Sensitivity and Wide Linearity. *Nanoscale* **2015,** 7, 8636-8644.

(46) Oh, J.; Kim, J. O.; Kim, Y.; Choi, H. B.; Yang, J. C.; Lee, S.; Pyatykh, M.; Kim, J.; Sim, J. Y.; Park, S. Highly Uniform and Low Hysteresis Piezoresistive Pressure Sensors Based on Chemical Grafting of Polypyrrole on Elastomer Template with Uniform Pore Size. *Small* **2019,** 15, 1901744.

(47) Su, X.; Wu, X.; Chen, S.; Nedumaran, A. M.; Stephen, M.; Hou, K.; Czarny, B.; Leong, W. L. A Highly Conducting Polymer for Self-Healable, Printable, and Stretchable Organic Electrochemical Transistor Arrays and Near Hysteresis-Free Soft Tactile Sensors. *Adv. Mater.* **2022**, 2200682.

(48) Chang, S.; Li, J.; He, Y.; Liu, H.; Cheng, B. A High-Sensitivity and Low-Hysteresis Flexible Pressure Sensor Based on Carbonized Cotton Fabric. *Sens. Actuators, A* **2019,** 294, 45-53.

(49) Pyo, S.; Lee, J.; Bae, K.; Sim, S.; Kim, J. Recent Progress in Flexible Tactile Sensors for Human‐Interactive Systems: From Sensors to Advanced Applications. *Adv. Mater.* **2021,** 33, 2005902.

(50) Pan, L.; Chortos, A.; Yu, G.; Wang, Y.; Isaacson, S.; Allen, R.; Shi, Y.; Dauskardt, R.; Bao, Z. An Ultra-Sensitive Resistive Pressure Sensor Based on Hollow-Sphere Microstructure Induced Elasticity in Conducting Polymer Film. *Nat. Commun.* **2014,** 5, 3002.

(51) Gong, S.; Schwalb, W.; Wang, Y.; Chen, Y.; Tang, Y.; Si, J.; Shirinzadeh, B.; Cheng, W. A Wearable and Highly Sensitive Pressure Sensor with Ultrathin Gold Nanowires. *Nat. Commun.* **2014,** 5, 3132.

(52) Chen, X.; Liu, C.; Liu, S.; Lyu, B.; Li, D. A High Compressibility Pressure—Sensitive Structure Based on CB@ PU Yarn Network. *Sensors* **2018,** 18, 4141.

(53) He, Y.; Ming, Y.; Li, W.; Li, Y.; Wu, M.; Song, J.; Li, X.; Liu, H. Highly Stable and Flexible Pressure Sensors with Modified Multi-Walled Carbon Nanotube/Polymer Composites for Human Monitoring. *Sensors* **2018,** 18, 1338.

(54) Gao, Y.; Yan, C.; Huang, H.; Yang, T.; Tian, G.; Xiong, D.; Chen, N.; Chu, X.; Zhong, S.; Deng, W.; Fang, Y.; Yang, W. Microchannel-Confined MXene Based Flexible Piezoresistive Multifunctional Micro-Force Sensor. *Adv. Funct. Mater.* **2020,** 30, 1909603.

(55) Huang, Y.-P.; Liu, Y.-Y.; Hsu, W.-H.; Lai, L.-J.; Lee, M. S. Monitoring and Assessment of Rehabilitation Progress on Range of Motion After Total Knee Replacement by Sensor-Based System. *Sensors* **2020,** 20, 1703.

(56) Majumder, S.; Mondal, T.; Deen, M. J. Wearable Sensors for Remote Health Monitoring. *Sensors* **2017,** 17, 130.

(57) Alaskar, H.; Jaafar Hussain, A. In Data Mining To Support the Discrimination of Amyotrophic Lateral Sclerosis Diseases Based on Gait Analysis, Intelligent Computing Methodologies: 14th International Conference, ICIC 2018, Wuhan, China, August 15-18, 2018, Proceedings, Part III 14, Springer: 2018; pp 760-766.

(58) Cicek, M. O.; Doganay, D.; Durukan, M. B.; Gorur, M. C.; Unalan, H. E. Seamless Monolithic Design for Foam Based, Flexible, Parallel Plate Capacitive Sensors. *Advanced Materials Technologies* **2021,** 6, 2001168.

(59) Perry, B. J.; Stipancic, K. L.; Martino, R.; Plowman, E. K.; Green, J. R. Biomechanical Biomarkers of Tongue Impairment During Swallowing in Persons Diagnosed with Amyotrophic Lateral Sclerosis. *Dysphagia* **2021,** 36, 147-156.

(60) Pinto, S.; Quintarelli, S.; Silani, V. New Technologies and Amyotrophic Lateral Sclerosis – Which Step Forward Rushed by the COVID-19 Pandemic. *J. Neurol. Sci.* **2020,** 418, 117081.

(61) Fu, Y.; Zhao, S.; Wang, L.; Zhu, R. A Wearable Sensor Using Structured Silver-Particle Reinforced PDMS for Radial Arterial Pulse Wave Monitoring. *Adv. Healthcare Mater.* **2019,** 8, 1900633.

(62) Chirinos, J.; Kips, J.; Roman, M.; Medina-Lezama, J.; Li, Y.; Woodiwiss, A.; Norton, G.; Yasmin, L. Van Bortel, JG Wang, JR Cockcroft, RB Devereux, IB Wilkinson, P. Segers, CM McEniery. *Hypertension* **2011,** 57, 1108.

(63) Yi, Z.; Liu, Z.; Li, W.; Ruan, T.; Chen, X.; Liu, J.; Yang, B.; Zhang, W. Piezoelectric Dynamics of Arterial Pulse for Wearable Continuous Blood Pressure Monitoring. *Adv. Mater.* **2022**, 2110291.

(64) Yang, J. C.; Mun, J.; Kwon, S. Y.; Park, S.; Bao, Z.; Park, S. Electronic Skin: Recent Progress and Future Prospects for Skin-Attachable Devices for Health Monitoring, Robotics, and Prosthetics. *Adv. Mater.* **2019,** 31, 1904765.

TOC figure

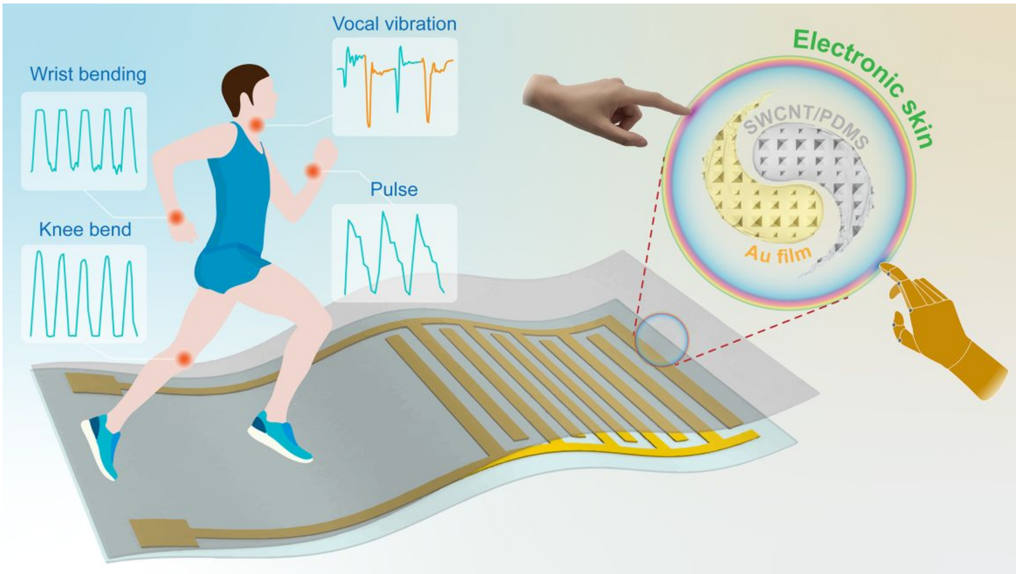
Vocal vibration
Wrist bending
Pulse
Knee bend
Electronic skin
SWCNT/PDMS
Au film